Rotational sequences in N = 98 167Tm populated in the 164Dy(7Li, 4nγ) 167Tm fusion-evaporation reaction

M. J. Burns, R. Chapman, K. M. Spohr, J. Ollier, M. Labiche, X. Liang, Y. Sun, Yan-Xin Liu, E. Farnea, M. Axiotis, T. Martinez, D. R. Napoli, C. Ur, and Th. Kröll

Rotational sequences in $N = 98$ ^{167}Tm populated in the ^{164}Dy(^{7}Li, $4n\gamma$) ^{167}Tm fusion-evaporation reaction

M. J. Burns,[1,2,*] R. Chapman [1,2,†] K. M. Spohr [1,2,‡] J. Ollier,[1,2,§] M. Labiche,[1,2,‖] X. Liang,[1,2] Y. Sun [3] Yan-Xin Liu,[4]
E. Farnea,[5,¶] M. Axiotis [5] T. Martinez [5,#] D. R. Napoli [5] C. Ur,[6,‡] and Th. Kröll [6,**]

[1]*School of Computing, Engineering, and Physical Sciences, University of the West of Scotland, Paisley PA1 2BE, United Kingdom*
[2]*The Scottish Universities Physics Alliance (SUPA), United Kingdom*
[3]*School of Physics and Astronomy, Shanghai Jiao Tong University, Shanghai 200240, People's Republic of China*
[4]*School of Science, Huzhou University, Huzhou 313000, People's Republic of China*
[5]*INFN, Laboratori Nazionali di Legnaro, I-35020 Legnaro, Padova, Italy*
[6]*INFN, Sezione di Padova, and Dipartimento di Fisica, Università di Padova, I35131 Padova, Italy*

High spin states in $^{167}_{69}$Tm$_{98}$ were studied using the ^{164}Dy(^{7}Li, $4n\gamma$) ^{167}Tm fusion-evaporation reaction. The XTU Tandem accelerator at the INFN Legnaro National Laboratory was used to accelerate a beam of ^{7}Li ions to 55 MeV, and γ rays from the evaporation residues were studied using the GASP Ge multidetector γ-ray array. The present data have allowed the $1/2^-$[541] yrast sequence of ^{167}Tm to be established to spin $61/2^-$, the $1/2^+$[411] ground-state band to be extended to $(51/2^+)$, and the $7/2^+$[404] and $7/2^-$[523] rotational sequences to be extended to spins $(43/2^+)$ and $(39/2^-)$, respectively. The experimental data have been compared with the results of cranked shell-model calculations; for the above decay sequences, crossing frequencies are in agreement with those of the neighboring even-even isotones, within experimental errors, and there is no evidence of a configuration-dependence of band crossing frequencies. Experimental $B(M1)/B(E2)$ values were extracted and compared with the results of theoretical calculations which are based on a semiclassical cranking model. Finally, the experimental high-spin decay sequences have been compared with the results of projected shell-model (PSM) calculations; agreement between experiment and theory is excellent over the complete range of spins. The calculated energy levels of the one-quasiparticle bands in ^{167}Tm depend sensitively on the deformation parameters used in the PSM calculation.

I. INTRODUCTION

The nucleus ^{167}Tm lies ten neutrons away from neutron number 88, where, for stable nuclei, a phase change takes place from spherical to deformed nuclear shapes. It sits in a region of stable nuclear ground-state quadrupole deformation

which is located in the rare-earth region with mass numbers in the range from 150 to 190. The odd-A isotopes of Tm with $A > 163$ have axially deformed nuclei [1–7], while the experimental evidence suggests that the lighter isotopes with $157 < A < 161$ are triaxial [8–12]. It is therefore to be expected that the nuclear level scheme of ^{167}Tm will be composed of rotational bands built on the odd quasiproton which, near the fermi surface, can occupy the Nilsson configurations, principally $1/2^+$[411], $3/2^+$[411], $5/2^+$[402], $7/2^+$[404], $1/2^-$[541], and $7/2^-$[523]. With increasing rotational frequency of the nucleus, the effect of the Coriolis force on nucleon motion, for this mass region, is to break a pair of high-j low-Ω quasineutrons based on the $i_{13/2}$ shell-model orbital; this results in the alignment of their total angular momentum along the direction of collective nuclear rotational angular momentum. In this way, the nucleus is able to generate increasing angular momentum more effectively than by increasing its rotational angular momentum. At the critical rotational frequency corresponding to pair alignment, an increase in quasiparticle angular momentum is therefore observed. The interest in studying the high-spin states of an odd-Z nucleus in this region of the nuclear chart is to determine the nature of the band crossing between the one- and three-quasiparticle rotational sequences and to compare

———

*Present address: Los Alamos National Laboratory, P.O. Box 1663, Los Alamos, NM 87545, USA.

†Robert.Chapman@uws.ac.uk

‡Present address: Extreme Light Infrastructure (ELI-NP) & IFIN-HH, Horia Hulubei National Institute of Physics and Nuclear Engineering, Bucharest-Măgurele, RO-077125, Romania.

§Present address: Rapiscan Systems, Prospect Way, Victoria Business Park, Biddulph, Stoke-on-Trent ST8 7PL, United Kingdom.

‖Present address: STFC Daresbury Laboratory, Daresbury, Warrington WA4 4AD, United Kingdom.

¶Deceased.

#Present address: CIEMAT (Centro de Investigaciones Energeticas, MedioAmbientales y Tecnologicas), Avenida Complutense 40, E-28040 Madrid, Spain.

**Present address: Institut für Kernphysik, Technische Universität Darmstadt, 64289 Darmstadt, Germany.

the observed characteristics of the crossing phenomenon with those of the neighboring isotopes and the even-even isotones. Under certain circumstances, the odd quasiparticle has a major impact on the rotational frequency ($\hbar\omega_c$) at which the alignment of a pair of $i_{13/2}$ quasineutrons occurs. The addition of a single quasiparticle to an even-even core may have a significant effect on the crossing frequency depending on whether the nucleon is a neutron or a proton and on the particular Nilsson configuration ($\Omega^{\pi}[Nn_z\Lambda]$) occupied; quasiparticle blocking by the odd nucleon and deformation-driving effects are, in this respect, two areas of interest.

The nucleus ^{167}Tm, with $N = 98$, lies at a peak of interaction strength [13] between the ground-state band and that based on the neutron $i_{13/2}$ two-quasiparticle configuration; this is a consequence of the deformed shell gap at neutron number $N = 98$. The neighboring even-even isotones, ^{166}Er [14] and ^{168}Yb [15], are known to exhibit a gradual upbend in the behavior of the quasiparticle alignment as a function of rotational frequency. The nucleus ^{167}Tm presents an excellent opportunity to study these effects. Previous publications [1–5] have established rotational sequences based on a number of Nilsson configurations to spin values just below the two $i_{13/2}$ quasineutron crossing regime. A preliminary report of the present work was previously published [14].

II. EXPERIMENTAL METHODS

High spin states of ^{167}Tm were populated using the ^{164}Dy(^{7}Li, $4n\gamma$)^{167}Tm fusion-evaporation reaction. The HVEC XTU Tandem Van de Graaff accelerator at the INFN, Legnaro National Laboratory, Italy was used to accelerate ^{7}Li ions to 55 MeV, which were then incident on an isotopically enriched ^{164}Dy (95.6%) target of thickness 3.5 mg cm^{-2}. The fusion-evaporation channels corresponding to the emission of four, five, and six neutrons were dominant in the data, leading to the population of ^{167,166,165}Tm, respectively. The estimated cross section for the $4n$ reaction channel leading to ^{167}Tm was ≈ 20 mb (approximately 1.3% of the total fusion cross section), corresponding to $\approx 5 \times 10^9$ events. The rotational sequences of ^{165,166}Tm have been studied previously to high spin [1–5]; in the present experiment, it was not possible to extend the decay sequences further. ^{167}Tm, on the other hand, has not been studied since the early 1980s, with the exception of the work by Jensen *et al.* [16], in which the rotational sequence based on the $\pi h_{9/2}$[541]1/2$^-$ bandhead was extended to spin 61/2$^-$. In the present work, it was possible to extend the other decay sequences to higher spins than previously reported.

Gamma rays emitted from the final nuclei populated in the reaction were detected using the GASP (GAmma-ray SPectrometer) array of 40 escape-suppressed hyperpure n-type germanium (HPGe) detectors and an 80 element inner bismuth germanate (BGO) ball, which acts as a multiplicity filter and total energy spectrometer [17,18]. The average Ge energy resolution at 1332 keV was better than 2.3 keV FWHM and the relative efficiency of each crystal was about 80%. The high efficiency and resolving power of the GASP array yielded good statistics for γ-γ-γ triples events. The trigger conditions for an "event" corresponded to two or more Ge

signals and two or more BGO inner-ball element signals. The Ge data were subsequently gain matched and sorted into a γ-γ-γ cube using the sort code GAVSORT [19]. The cube was analysed using programs from the RADWARE [20] analysis package. γ-ray coincidence spectra were created initially by gating on previously known transitions belonging to ^{167}Tm [16,21]. Relative γ-ray detection efficiencies as a function of γ-ray energy for the Ge detectors were measured using standard radioactive sources of ^{133}Ba and ^{152}Eu.

III. RESULTS

Prior to the present experiment, the band structure of the ^{167}Tm nucleus was studied by Svensson *et al.* [22], Olbrich *et al.* [21], and Jensen *et al.* [16]. The ^{167}Er(p, $n\gamma$)^{167}Tm reaction was used by Svensson *et al.* [22] to study the level structure to a maximum spin value of 21/2$\hbar$. Decay sequences based on states with the Nilsson configurations 1/2$^+$[411], 3/2$^+$[411], 5/2$^+$[402], 7/2$^+$[404], 1/2$^-$[541], 7/2$^-$[523], and 9/2$^-$[514] were populated and γ-ray spectra in singles and in coincidence were measured with Ge(Li) and low-energy photon spectrometer (LEPS) detectors. An electron-electron coincidence spectrometer was used to measure the lifetimes of two levels in the ground band. Olbrich *et al.* [21] used the ^{165}Ho(α, $2n\gamma$)^{167}Tm reaction to populate rotational sequences based on states with the Nilsson configurations 1/2$^+$[411], 3/2$^+$[411], 5/2$^+$[402], 7/2$^+$[404], 1/2$^-$[541], 3/2$^-$[532] + {1/2$^-$[541]; K-2}, and 7/2$^-$[523]. The maximum angular momentum of populated states was 31/2$\hbar$. Singles and coincidence spectra were measured; two Ge(Li) detectors were used for the γ-γ coincidence measurements. More recently, Jensen *et al.* [16] populated high-spin states of ^{167}Tm using the ^{124}Sn(^{48}Ca, $p4n$)^{167}Tm fusion-evaporation reaction; the favored signature of the 1/2$^-$[541] rotational sequence was extended to spin 61/2. No new transitions were added to the unfavored signature of the band. The EUROGAM γ-ray array of 45 escape-suppressed Ge detectors was used in the work. The most recent Nuclear Data Sheets compilation for $A = 167$ was published in 2000 [23] and predates the work of Burns *et al.* [14], a preliminary publication of the present work.

Figure 1 presents the decay sequences of ^{167}Tm based on this work. The level scheme presented here was based on γ-ray coincidence measurements and on transition intensity considerations. Spins and parities of previously unobserved levels have been tentatively assigned on the assumptions that, within each rotational sequence, there is no change of parity and that the spin value increases as expected with increasing excitation energy. Thus, proposed spin and parity assignments should be regarded as tentative and are consequently presented here in parentheses.

The in-band transitions previously observed [21] for the ground-state rotational sequence, based on the Nilsson configuration 1/2$^+$[411], have been confirmed in the present work and the two decay sequences corresponding to the favored and unfavored signatures of the band have been extended to spins (51/2$^+$) and (45/2$^+$), respectively. Figure 2(a) shows the γ-ray spectrum corresponding to a sum of all double gates involving the previously known γ-ray transitions at energies
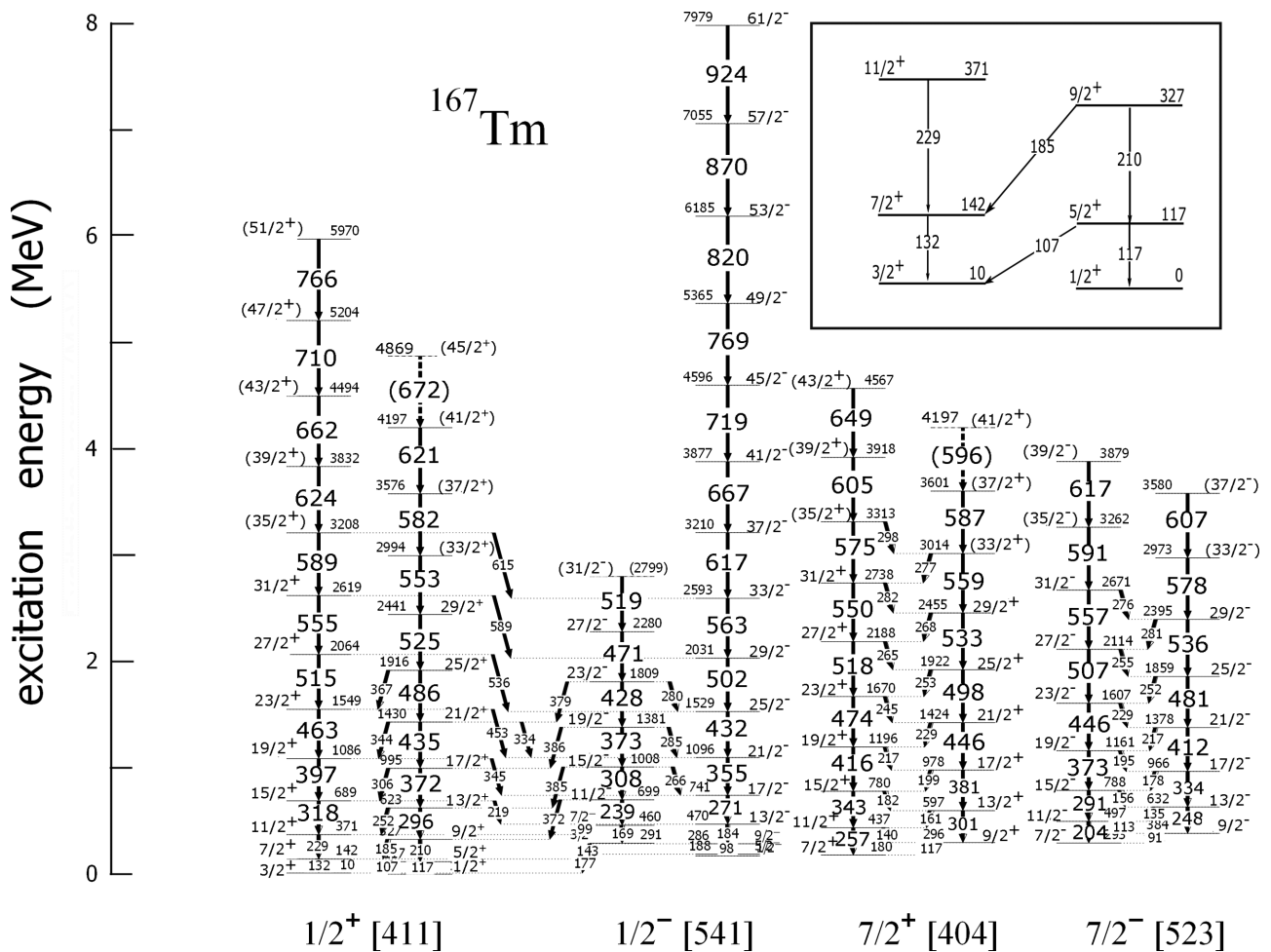
FIG. 1. Level scheme of ^{167}Tm from the present work. The inset shows the bottom few states of the $1/2^+$[411] decay sequence. Energies are in units of keV. The figure was adapted from Ref. [14]. A more detailed presentation of the low spin members of the rotational sequences is given in Refs. [21,22].

of 132, 229, 318, 397, 463, and 515 keV. Three of the five new γ-ray transitions for the $\alpha = -\frac{1}{2}$ signature partner of the band, above the already established $31/2^+$ state at 2619 keV, can be clearly seen at energies of 589, 624, and 662 keV, corresponding to the deexcitation of the $(35/2^+)$, $(39/2^+)$, and $(43/2^+)$ states, respectively. The inset to Fig. 2(a) shows a γ-ray spectrum corresponding to a double gate set on γ-ray peaks at energies of 624 and 662 keV; two further transitions at energies of 710 and 766 keV can be observed, corresponding to the deexcitation of the $(47/2^+)$ and $(51/2^+)$ states, respectively. Three new levels have also been added to the $\alpha = \frac{1}{2}$ signature partner, corresponding to the deexcitation of the $(33/2^+)$, $(37/2^+)$, and $(41/2^+)$ levels via the 553-, 582-, and 621-keV γ-ray transitions, respectively. A further tentative addition to the band has been observed at an energy of 672 keV; it is proposed here that this transition corresponds to the depopulation of the $(45/2^+)$ state. The new transitions can be seen in the gamma-ray spectrum of Fig. 2(b), which corresponds to a double gate set on the 372- and 525-keV transitions. The lowest lying transitions within the band of signature $\alpha = -\frac{1}{2}$, corresponding to the decay of the 142-keV $(7/2^+)$ and 371-keV $(11/2^+)$ states (see also inset to Fig. 1)

can also be seen at energies of 132 and 229 keV, respectively [marked $*$ in Fig. 2(b)]; the crossing transitions at energies of 185 and 252 keV [marked $\times$ in Fig. 2(b)] can also be seen in the spectrum. The inset to Fig. 2(b) shows a γ-ray spectrum resulting from a double gate set on the 486- and 582-keV transitions, and this provides further evidence for the new high-spin states populated in the rotational sequence. The extensions to the $1/2^+$[411] decay sequence were based on these and on similar double-gated γ-ray spectra. The $\alpha = +1/2$ to $\alpha = -1/2$ transitions of energy 107, 185, 252, and 306 keV were previously assigned $(M1 + E2)$ multipolarity with small mixing ratio [23]. No multipolarity assignments have been made for the previously observed 344- and 367- keV transitions. The low energy $\alpha = -1/2$ to $\alpha = +1/2$ transitions of energy 10.45 keV $(3/2^+ \longrightarrow 1/2^+)$, 25.8 keV $(7/2^+ \longrightarrow 5/2^+)$, 44.5 keV (uncertain placement $11/2^+ \longrightarrow 9/2^+$), and 67.0 keV $(15/2^+ \longrightarrow 13/2^+)$ [23] have not been observed in the present work. The 10.4-keV transition is very heavily converted $(\alpha \approx 650)$ [23].

The previously observed interband transitions from levels of the the $\alpha = -1/2$ signature of the $1/2^+$[411] band to levels of the $\alpha = +1/2$ signature of the $1/2^-$[541] band at
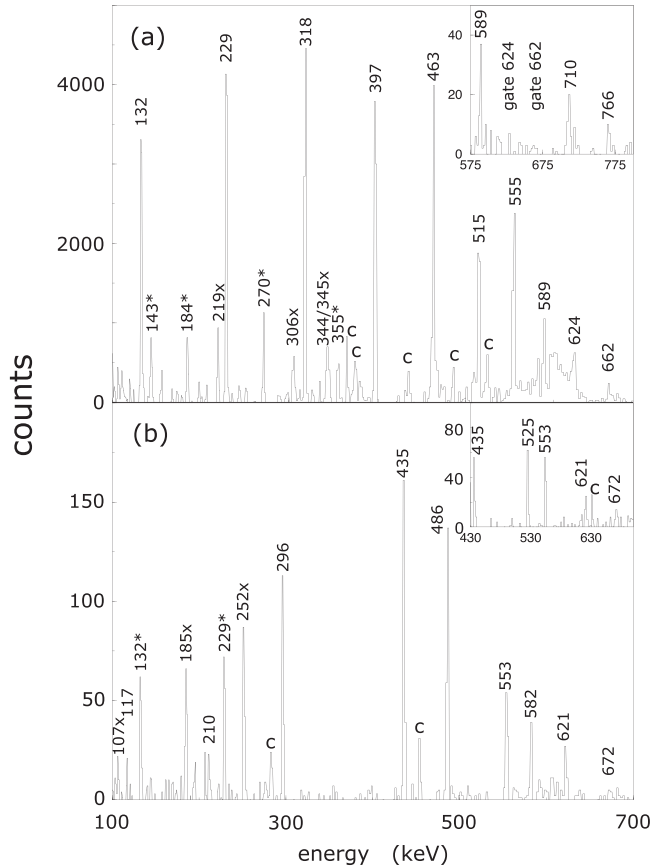
FIG. 2. Examples of γ-ray spectra corresponding to double gates on known transitions depopulating levels of the $1/2^+[411]$ band in ^{167}Tm. (a) The γ-ray spectrum corresponding to a sum of all double gates involving the previously known γ-ray transitions at energies of 132, 229, 318, 397, 463, and 515 keV. The inset shows a γ-ray spectrum corresponding to a double gate set on γ-ray photopeaks at energies of 624 and 662 keV. (b) The γ-ray spectrum corresponding to a double gate at γ-ray energies of 372 and 525 keV. The inset to the figure shows a γ-ray spectrum resulting from a double gate set on the 486- and 582-keV transitions. See text for details.

energies of 218.9, 345.2, 453.8, 536.7, and 589.5 keV have been observed in the present work. The 85.1-keV $11/2^+$ to $9/2^-$ transition was not seen here.

The favored signature of the $1/2^-[541]$ rotational sequence was extended by Jensen *et al.* [16] to spin $61/2^-$ and a tentative transition, of energy 922 keV, corresponding to the $65/2^- \longrightarrow 61/2^-$ transition, was proposed. Here, it was not possible to extend the $\alpha = \frac{1}{2}$ signature of the band to higher spin. As in the study of Olbrich *et al.* [21], the rotational sequence with signature $\alpha = -\frac{1}{2}$ was very weakly populated; in the present work it was identified up to the previously known $(31/2^-)$ state, but not beyond.

All the states populated in the $7/2^+[404]$ rotational sequence up to spin $31/2^+$ conform with the previous work of Olbrich *et al.* [21] (see Fig. 1). The rotational sequence corresponding to the $\alpha = -\frac{1}{2}$ signature has been extended to spin $(43/2^+)$ by the addition of three new levels of proposed spin $(35/2^+)$, $(39/2^+)$, and $(43/2^+)$. The γ-ray spectrum of

Fig. 3(a), which corresponds to a double gate on the γ-ray photopeaks at energies of 518 and 550 keV, shows the new transitions at the photopeak energies of 575, 605, and 649 keV. The signature partner ($\alpha = \frac{1}{2}$) has been extended to spin $(37/2^+)$ by the addition of two new levels, at energies of 3014 and 3601 keV. A further tentative transition of energy 596 keV, corresponding to the $(41/2^+) \longrightarrow (37/2^+)$ transition, has been added to the decay scheme. Gamma-ray transitions within the rotational sequence can be seen in the spectrum of Fig. 3(b), which corresponds to a double gate at γ-ray energies of 301 and 498 keV.

The intensities of the $E2$ transitions within the decay sequences corresponding to both signatures of the rotational band based on the $7/2^-[523]$ orbital were very weak. On the other hand, the $M1$ interband transitions are relatively strong. Figure 3(c) shows a spectrum corresponding to a sum of double gates on all of the previously known $M1$ band-crossing transitions (91, 113, 135, 156, 178, 195, 217, 229, 252, 255, and 281 keV). The level sequence up to spin $31/2^-$ is in agreement with that of Olbrich *et al.* [21]. Two new transitions at energies of 591 and 617 keV have been added to the decay sequences corresponding to the $\alpha = -\frac{1}{2}$ signature of the band, which increases the level sequence to spin $(39/2^-)$. The transitions can be seen in Fig. 3(c). Two new transitions at energies of 578 and 607 keV have also been added to the $\alpha = \frac{1}{2}$ signature of the band, raising the known maximum spin to $(37/2^-)$ [see Fig. 3(c)].

The γ-ray transitions in the $1/2^+[411]$, $1/2^-[541]$, $7/2^+[404]$, and $7/2^-[523]$ rotational sequences of ^{167}Tm were ordered according to their relative intensities as shown in Tables I–IV, respectively; the relative intensities and spin assignments for the populated bands and their corresponding interband transitions are shown. Table V presents the measured relative γ-ray transition intensities for the interband transitions which connect the $1/2^+[411]$ and the $1/2^-[541]$ rotational sequences. Relative γ-ray intensities were obtained from spectra produced by setting double gates on transitions lower in the rotational sequence than those to be measured. Consequently, the relative intensities of the lowest transitions in each decay sequence cannot be accurately evaluated. In such cases, no relative intensities are recorded in the tables. In addition, some of the lowest energy photopeaks are challenging to observe; in these cases, relative γ-ray intensities do not appear in the tables. Quoted γ-ray intensities are those relative to the intensity of the 184-keV γ-ray transition, set at 1000 units.

IV. DISCUSSION

Experimental Routhians and aligned angular momenta, i_x, plotted as a function of rotational frequency, $\hbar\omega$, are presented in Figs. 4–6 for the rotational sequences populated in ^{167}Tm. A reference band has been subtracted with Harris parameters $J^0 = 35.5 \ \hbar^2 \mathrm{MeV}^{-1}$ and $J^1 = 118 \ \hbar^4 \mathrm{MeV}^{-3}$ [24]. Upbends in the alignment plots are, as usual, interpreted as arising from band crossings. As noted above, in this region of the periodic table, the rare-earth region, the first observed backbend or upbend is attributed to the alignment of a pair of $i_{13/2}$ neutrons and thus, in the present case, each one-quasiproton decay
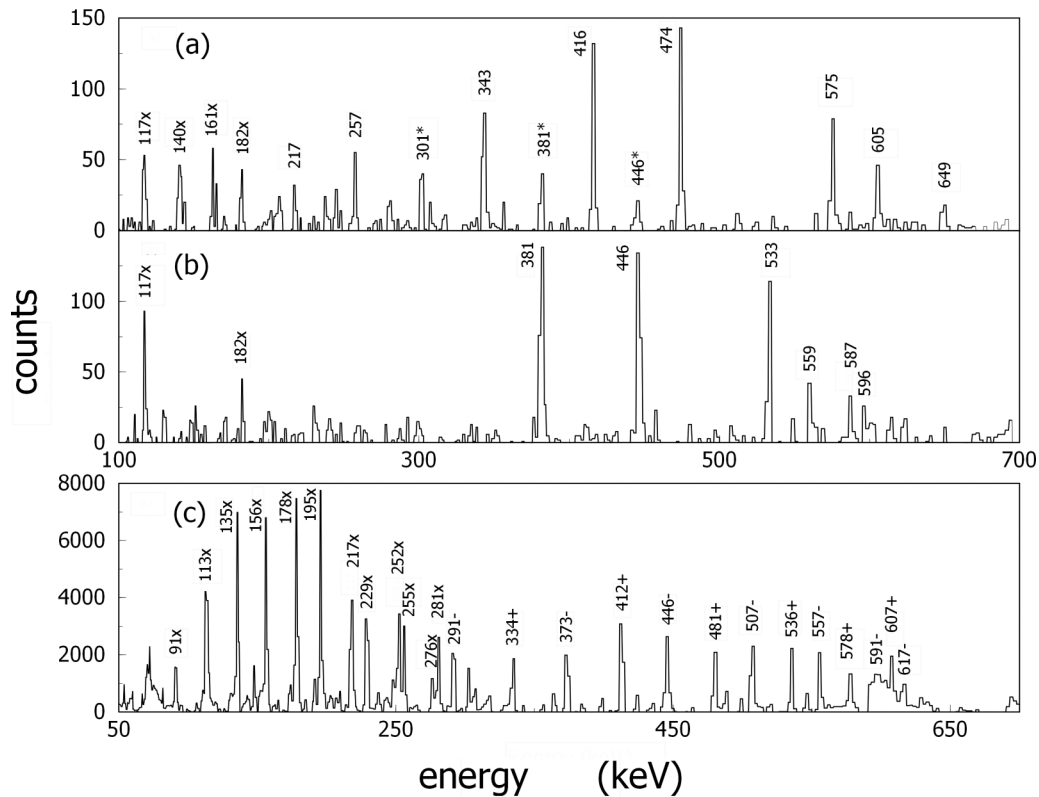
FIG. 3. Examples of γ-ray spectra corresponding to double gates on known transitions depopulating levels of the $7/2^+[404]$ band [spectra (a) and (b)] and of the $7/2^-[523]$ band [spectrum (c)] in ^{167}Tm. The γ-ray spectra are presented which correspond to (a) a double gate on the γ-ray photopeaks at energies of 518 and 550 keV in the $7/2^+[404]$ band, (b) a double gate at γ-ray energies of 301 and 498 keV in the $7/2^+[404]$ band, and (c) a sum of double gates on all previously known $M1$ band-crossing transitions in the $7/2^-[523]$ band. Peaks labeled with an $\times$ correspond to cross-band transitions whereas peaks labeled $+/-$ correspond to $E2$ transitions within the $\alpha = +\frac{1}{2}$ and $\alpha = -\frac{1}{2}$ decay sequences, respectively.

sequence is crossed by a three-quasiparticle decay sequence. In the cranked shell-model (CSM) terminology, this is denoted as the AB crossing [25,26]. Crossing frequencies, $\hbar\omega_c$, and gains in aligned angular momenta, Δi_x, for the crossings observed in the bands here are listed in Table VI, together with the corresponding values for the neighboring even-even $Z = 68$ and $Z = 70$ isotones, ^{166}Er [14] and ^{168}Yb [15], respectively.

A. The ground-state band ($1/2^+[411]$)

The $1/2^+[411]$ bandhead is based, at zero deformation, on the single $2d_{3/2}$ quasiproton. The experimental Routhians for the two decay sequences of the rotational band, Fig. 4(a), show a signature splitting at low rotational frequencies and an increase in splitting as a function of rotational frequency. However, the aligning $i_{13/2}$ quasineutrons have the effect of reducing the splitting at high rotational frequencies. As a consequence of the splitting in the Routhians, the two signatures of the rotational sequence cross the three-quasiparticle configuration at different rotational frequencies. The $\alpha = \frac{1}{2}$ signature crosses first, at a frequency of 250(3) keV, while the $\alpha = -\frac{1}{2}$ signature crosses at a frequency of 270(3) keV. Experimental quasiparticle alignments, band crossing frequencies,

and signature splittings were compared with the results of cranked shell-model calculations. The values of the quadrupole and hexadecapole deformation parameters $(\epsilon_2, \epsilon_4) = (0.26, 0.013)$ used in the CSM calculations were taken from the Lund systematics [28], calculated as described in Ref. [29], and the pairing gap parameter, Δ, calculated from atomic masses [30], was multiplied by a factor of 0.8 to account, in an approximate way, for the effect of nuclear rotation on the pairing field at high rotational frequencies. The experimental crossing frequencies are consistent with results obtained from CSM calculations, namely $\hbar\omega_c = 265(10)$ keV; the quasiproton does not block the aligning $i_{13/2}$ neutrons. In the Nilsson diagram, the energy of the $1/2^+[411]$ proton orbital as a function of quadrupole deformation has no slope and there are consequently no deformation-driving effects. The initial alignment, Fig. 4(b), due to the single quasiproton can be seen to be $0\hbar$ for the $\alpha = \frac{1}{2}$ signature and $0.6\hbar$ for the $\alpha = -\frac{1}{2}$ signature of the rotational sequence. These results compare well with results of CSM calculations, namely an initial alignment ($i_x = -de'/d\hbar\omega$) of $0\hbar$ for the $\alpha = \frac{1}{2}$ signature and $1\hbar$ for the $\alpha = -\frac{1}{2}$ signature of the band. The average crossing frequency agrees well with that of the yrast sequences in the neighbouring even-even isotones, ^{166}Er and ^{168}Yb, see Table VI. The measured gain in quasiparticle

TABLE I. Relative γ-ray intensities and spin assignments of all observed transitions in the $1/2^+[411]$ rotational sequence of ^{167}Tm. The uncertainty in γ-ray energies is 1 keV. See text for details.

E_γ (keV)	J_i^π	J_f^π	Relative intensity
117	$5/2^+$	$1/2^+$	
210	$9/2^+$	$5/2^+$	
296	$13/2^+$	$9/2^+$	
372	$17/2^+$	$13/2^+$	17.4(5)
435	$21/2^+$	$17/2^+$	13.0(5)
486	$25/2^+$	$21/2^+$	11.0(9)
525	$29/2^+$	$25/2^+$	8.14(70)
553	$(33/2^+)$	$29/2^+$	2.74(16)
582	$(37/2^+)$	$(33/2^+)$	1.73(12)
621	$(41/2^+)$	$(37/2^+)$	1.54(11)
132	$7/2^+$	$3/2^+$	
229	$11/2^+$	$7/2^+$	
318	$15/2^+$	$11/2^+$	60.8(11)
397	$19/2^+$	$15/2^+$	39.6(9)
463	$23/2^+$	$19/2^+$	22.7(7)
515	$27/2^+$	$23/2^+$	16.7(7)
555	$31/2^+$	$27/2^+$	14.4(6)
589	$(35/2^+)$	$31/2^+$	9.92(53)
624	$(39/2^+)$	$(35/2^+)$	3.77(23)
662	$(43/2^+)$	$(39/2^+)$	1.51(5)
710	$(47/2^+)$	$(43/2^+)$	0.61(5)
766	$(51/2^+)$	$(47/2^+)$	0.12(1)
107	$5/2^+$	$3/2^+$	
185	$9/2^+$	$7/2^+$	
252	$13/2^+$	$11/2^+$	26.5(9)
306	$17/2^+$	$15/2^+$	15.3(9)
344	$21/2^+$	$19/2^+$	7.97(54)
367	$25/2^+$	$23/2^+$	2.81(22)

TABLE II. Relative γ-ray intensities and spin assignments of all observed transitions in the $1/2^-[541]$ rotational sequence of ^{167}Tm. The uncertainty in γ-ray energies is 1 keV. See text for details.

E_γ (keV)	J_i^π	J_f^π	Relative intensity
98	$9/2^-$	$5/2^-$	
184	$13/2^-$	$9/2^-$	1000(13)
271	$17/2^-$	$13/2^-$	461(6)
355	$21/2^-$	$17/2^-$	336(3)
432	$25/2^-$	$21/2^-$	231(3)
502	$29/2^-$	$25/2^-$	140(2)
563	$33/2^-$	$29/2^-$	81(2)
617	$37/2^-$	$33/2^-$	67(2)
667	$41/2^-$	$37/2^-$	27(1)
719	$45/2^-$	$41/2^-$	21.5(7)
769	$49/2^-$	$45/2^-$	6.70(6)
820	$53/2^-$	$49/2^-$	1.88(4)
870	$57/2^-$	$53/2^-$	0.42(3)
924	$61/2^-$	$57/2^-$	0.24(2)
169	$7/2^-$	$3/2^-$	
239	$11/2^-$	$7/2^-$	
308	$15/2^-$	$11/2^-$	
373	$19/2^-$	$15/2^-$	
428	$23/2^-$	$19/2^-$	
471	$27/2^-$	$23/2^-$	
519	$(31/2^-)$	$27/2^-$	
266	$15/2^-$	$17/2^-$	
285	$19/2^-$	$21/2^-$	
280	$23/2^-$	$25/2^-$	

alignment is about $\approx 4.5\hbar$ for the $\alpha = -\frac{1}{2}$ signature and $\approx 5.5\hbar$ for the $\alpha = \frac{1}{2}$ signature of the band. These values are less than that predicted by the cranked shell model, namely $7\hbar$. Crossing frequencies of the $1/2^+[411]$ decay sequences in ^{165}Tm, ^{167}Tm, and ^{169}Tm were interpreted by Asgar *et al.* [7] within the context of the cranked shell model approach by calculating the total Routhian surfaces, crossing frequencies, and interaction strengths for these nuclei; the gradual decrease in crossing frequency with increasing Tm mass number, from 0.29 to 0.24 MeV, is very well reproduced by calculation.

B. $1/2^-[541]$ rotational sequence

In the present work, no extensions were made to the $1/2^-[541]$ rotational sequence established by Jensen *et al.* [16]. While most rotational bands in odd-Z nuclei in the rare earth region have the first band-crossing frequencies and quasiparticle alignments similar to those in the neighboring even-even isotones, the first band crossing in the $1/2^-[541]$ band, which is based at zero deformation on the spherical $\pi h_{9/2}$ proton orbital, is shifted to higher frequencies, with a smaller gain in aligned angular momentum. However, as discussed by Jensen *et al.* [16], the behavior of the band in $N = 98$ ^{167}Tm is quite different; the shift in crossing frequency,

while still larger than in the neighboring even-even isotones, see Table VI, is much smaller than in odd-Z nuclei with $N \neq 98$. In contrast, the $N = 98$ nuclei exhibit, in relation to quasiparticle alignment, the largest discrepancy between odd-Z nuclei and the neighboring even-even isotones. The reduction in quasiparticle alignment at $N = 98$ appears to be a unique feature of the $1/2^-[541]$ intruder orbital.

C. $7/2^+[404]$ rotational sequence

The $7/2^+[404]$ rotational sequence is based on a single quasiproton originating from the $1g_{7/2}$ spherical shell. Since the orbital is considerably upwards sloping for a prolate nucleus, the effect of occupancy is to reduce the nuclear quadrupole deformation (if the nucleus is soft enough to respond) and this, in turn, would lead to a reduction in the rotational frequency required to align a pair of $i_{13/2}$ quasineutrons.

The experimental Routhians, Fig. 5(a), show that the crossing frequency is 258(2) keV, which is in reasonable agreement with the experimental value for the even-even ^{166}Er core, namely 262(2)keV [27]; deformation-driving effects therefore appear to be insignificant here. The initial quasiparticle alignment i_x is $0.30(8)\hbar$, Fig. 5(b); this result compares well with CSM results of $0.33\hbar$. The CSM results show a complete alignment gain of $7\hbar$. In the quasiparticle alignment plot, Fig. 5(b), there is an alignment gain of approximately $6\hbar$.

TABLE III. Relative γ-ray intensities and spin assignments of all observed transitions in the $7/2^+$[404] rotational sequence of ^{167}Tm. The uncertainty in γ-ray energies is 1 keV. See text for details.

E_γ (keV)	J_i^π	J_f^π	Relative intensity
257	$11/2^+$	$7/2^+$	
343	$15/2^+$	$11/2^+$	
416	$19/2^+$	$15/2^+$	5.82(18)
474	$23/2^+$	$19/2^+$	3.17(8)
518	$27/2^+$	$23/2^+$	2.47(8)
550	$31/2^+$	$27/2^+$	1.01(4)
575	$(35/2^+)$	$31/2^+$	0.83(5)
605	$(39/2^+)$	$(35/2^+)$	0.62(4)
649	$(43/2^+)$	$(39/2^+)$	0.14(1)
301	$13/2^+$	$9/2^+$	
381	$17/2^+$	$13/2^+$	
446	$21/2^+$	$17/2^+$	10.0(3)
498	$25/2^+$	$21/2^+$	4.43(16)
533	$29/2^+$	$25/2^+$	2.45(12)
559	$(33/2^+)$	$29/2^+$	1.46(10)
587	$(37/2^+)$	$(33/2^+)$	0.85(8)
117	$9/2^+$	$7/2^+$	
140	$11/2^+$	$9/2^+$	
161	$13/2^+$	$11/2^+$	
182	$15/2^+$	$13/2^+$	
199	$17/2^+$	$15/2^+$	
217	$19/2^+$	$17/2^+$	3.87(18)
229	$21/2^+$	$19/2^+$	1.08(6)
245	$23/2^+$	$21/2^+$	2.73(14)
253	$25/2^+$	$23/2^+$	0.49(5)
265	$27/2^+$	$25/2^+$	0.50(6)
268	$29/2^+$	$27/2^+$	0.20(2)
282	$31/2^+$	$29/2^+$	0.32(4)
277	$(33/2^+)$	$31/2^+$	0.12(2)
298	$(35/2^+)$	$(33/2^+)$	0.15(3)

TABLE IV. Relative γ-ray intensities and spin assignments of all observed transitions in the $7/2^-$[523] rotational sequence of ^{167}Tm. The uncertainty in γ-ray energies is 1 keV. See text for details.

E_γ (keV)	J_i^π	J_f^π	Relative intensity
204	$11/2^-$	$7/2^-$	
291	$15/2^-$	$11/2^-$	
373	$19/2^-$	$15/2^-$	
446	$23/2^-$	$19/2^-$	1.23(6)
507	$27/2^-$	$23/2^-$	1.14(6)
557	$31/2^-$	$27/2^-$	0.38(2)
591	$(35/2^-)$	$31/2^-$	0.14(1)
617	$(39/2^-)$	$(35/2^-)$	0.07(2)
248	$13/2^-$	$9/2^-$	
334	$17/2^-$	$13/2^-$	
412	$21/2^-$	$17/2^-$	12.3(5)
481	$25/2^-$	$21/2^-$	6.17(35)
536	$29/2^-$	$25/2^-$	3.54(22)
578	$(33/2^-)$	$29/2^-$	2.64(17)
607	$(37/2^-)$	$(33/2^-)$	2.09(22)
91	$9/2^-$	$7/2^-$	
113	$11/2^-$	$9/2^-$	
135	$13/2^-$	$11/2^-$	100(4)
156	$15/2^-$	$13/2^-$	37.4(21)
178	$17/2^-$	$15/2^-$	13.0(10)
195	$19/2^-$	$17/2^-$	5.19(32)
217	$21/2^-$	$19/2^-$	3.67(18)
229	$23/2^-$	$21/2^-$	4.29(19)
252	$25/2^-$	$23/2^-$	1.27(11)
255	$27/2^-$	$25/2^-$	1.01(10)
281	$29/2^-$	$27/2^-$	0.84(8)
276	$31/2^-$	$29/2^-$	0.43(7)

D. $7/2^-$[523] rotational sequence

The $7/2^-$[523] rotational sequence originates from the $1h_{11/2}$ spherical shell-model orbital at $\epsilon_2 = 0$. The experimental Routhians, Fig. 6(a), show no evidence of signature splitting, which is to be expected as the configuration is of high-j and high-Ω and therefore mixing with lower-Ω wave functions, as the rotational frequency increases, should be negligible. The slope (energy versus quadrupole deformation in the Nilsson diagram) of the $7/2^-$[523] Nilsson configuration is relatively flat; therefore we expect to see no deformation-driving effects on the crossing frequency. The CSM predicts a gain in alignment of $7\hbar$ for the two $i_{13/2}$ quasineutrons. Experimentally, an incomplete alignment gain ($\approx 3.5\hbar$) of about half this value is seen; see Fig. 6(b). The crossing frequency is, in this case, more difficult to determine from the Routhian as a consequence of the strong interaction between the one- and three-quasiparticle configurations; the Routhian is a smooth function of rotational frequency. In addition, the full alignment gain was not observed in the present work. The estimated crossing frequency of 250(10) keV is, within the quoted errors, in agreement with those of the even-even isotones. A previous study [3] of the $7/2^-$[523] rotational sequence in the neighboring nucleus $^{165}_{67}$Tm$_{92}$ has shown that the crossing frequency is slightly less than that of the even-even core ^{164}Er. There is a lack of high-spin data for rotational sequences based on the $7/2^-$[523] Nilsson configuration in the region around ^{167}Tm. However, in ^{159}Ho [31] the $\pi h_{11/2}$ decay sequence

TABLE V. Relative γ-ray intensities and spin assignments of all interband transitions between the $1/2^+$[411] and $1/2^-$[541] rotational sequences of ^{167}Tm. The uncertainty in γ-ray energies is 1 keV. See text for details.

E_γ (keV)	J_i^π	J_f^π	Relative intensity
219	$15/2^+$	$13/2^-$	
345	$19/2^+$	$17/2^-$	29.4(10)
453	$23/2^+$	$21/2^-$	14.2(7)
536	$27/2^+$	$25/2^-$	29.5(10)
589	$31/2^+$	$29/2^-$	22.6(11)
615	$(35/2^+)$	$33/2^-$	
334	$21/2^+$	$21/2^-$	
372	$11/2^-$	$9/2^+$	
385	$15/2^-$	$13/2^+$	
386	$19/2^-$	$17/2^+$	
379	$23/2^-$	$21/2^+$	

TABLE VI. Rotational frequencies, $\hbar\omega_c$, and gain in aligned angular momentum, Δi_x, at the AB-band crossing for rotational bands observed in ^{167}Tm, and for the yrast bands in the neighboring even-even isotones, ^{166}Er [27] and ^{168}Yb [15]. For the $1/2^-$[541] decay sequence, the values are those from Ref. [16].

Nucleus	$\Omega^\pi[Nn_z\Lambda]$	α	$\hbar\omega_c$ (keV)	Δi_x ($\hbar$)
^{167}Tm	$1/2^+$[411]	$+1/2$	250(3)	5.5
		$-1/2$	270(3)	4.5
	$1/2^-$[541]	$+1/2$	320(10)	2.4(4)
		$-1/2$		
	$7/2^+$[404]	$+1/2$	258(2)	6
		$-1/2$	258(2)	6
	$7/2^-$[523]	$+1/2$	250(10)	> 3.5
		$-1/2$	250(10)	> 3.5
^{166}Er	yrast band	0	262(2)	8.8(1)
^{168}Yb	yrast band	0	260(2)	9

FIG. 5. (a) Experimental Routhians and (b) quasiparticle alignment plotted as a function of rotational frequency for the decay sequences based on the $7/2^+$[404] Nilsson configuration. The full (empty) symbols represent the $\alpha = \frac{1}{2}$ ($-\frac{1}{2}$) signatures of the bands.

was observed to a frequency of about 0.35 MeV and a full alignment gain of $7.5\hbar$ observed. In this case, the crossing frequencies of 0.281 and 0.277 MeV for the $\alpha = -1/2$ and $\alpha = +1/2$ signatures of the rotational band, respectively, are in very good agreement with those of its neighboring isotone ^{166}Er ($\hbar\omega_c = 0.280$ MeV) [32]. Similarly, the quasiparticle alignment gains for the first band crossing in both nuclei are in good agreement. It would be helpful to extend this rotational sequence in ^{167}Tm well beyond the rotational frequency corresponding to the full alignment of the two $i_{13/2}$ quasineutrons.

E. $B(M1)/B(E2)$ ratios for the $7/2^-$[523] rotational sequence

Figure 7 presents experimental $B(M1)/B(E2)$ ratios as a function of spin $I(\hbar)$ for the $7/2^-$[523] rotational sequence. In the calculation of experimental $B(M1)/B(E2)$ values, the following expression was used:

$$\frac{B(M1, I \rightarrow I-1)}{B(E2, I \rightarrow I-2)} = 0.697 \frac{E_\gamma^5(E2)}{E_\gamma^3(M1)} \frac{1}{\lambda(1+\delta^2)} [\mu_N^2/e^2 b^2],$$
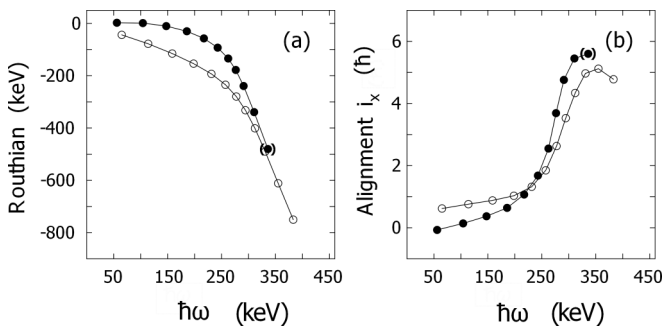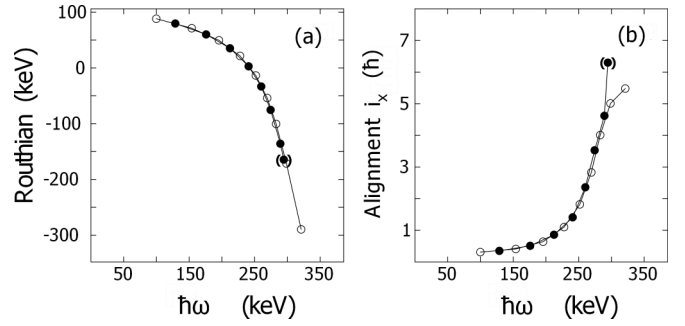
where the branching ratio $\lambda = T_\gamma(I \rightarrow I-2)/T_\gamma(I \rightarrow I-1)$ is obtained from the experimental γ-ray intensities. For the $7/2^-$[523] rotational sequence of ^{167}Tm, mixing ratios δ for transitions from states with $I < 21$ were measured by Olbrich *et al.* [21]; values of $|\delta|$ are small and reasonably constant at about 0.17 for the measured transitions. The effect of the mixing ratio on the experimental values of $B(M1)/B(E2)$ is therefore of the order of only 3 %. The experimental $B(M1)/B(E2)$ ratios can be seen to increase by around 60% at $I \approx 13$, see Fig. 7, and this is normally attributed to the effect of the alignment of two $i_{13/2}$ quasineutrons. The observed increase in $B(M1)/B(E2)$ ratio is attributed to an increase in the magnetic dipole transition probability. This effect has been observed previously in a number of neighboring rare earth odd-Z even-N isotopes, for example ^{165}Tm [1] and ^{165}Lu [35]. The component of magnetic moment perpendicular ($\mu_\perp$) to the total angular momentum vector (**I**) contributes significantly to the magnetic dipole transition rate and, as the two $i_{13/2}$ quasineutrons align, $\mu_\perp$ increases.

Theoretical $B(M1)/B(E2)$ ratios were calculated from the semiclassical cranking formula of Dönau and Frauendorf

FIG. 4. (a) Experimental Routhians and (b) quasiparticle alignment plotted as a function of rotational frequency for the decay sequences based on the $1/2^+$[411] Nilsson configuration. The full (empty) symbols represent the $\alpha = \frac{1}{2}$ ($-\frac{1}{2}$) signatures of the bands.
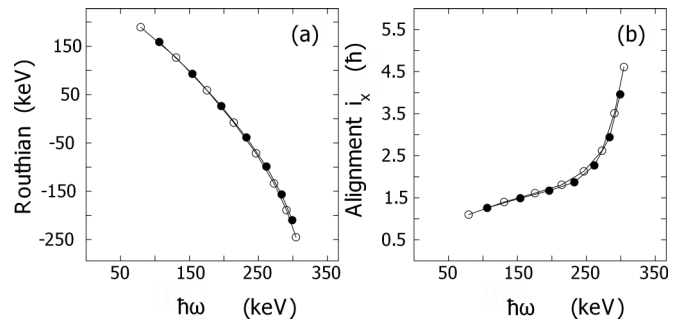

FIG. 6. (a) Experimental Routhians and (b) quasiparticle alignment plotted as a function of rotational frequency. The plots show rotational sequences based on the $7/2^-$[523] Nilsson configuration. The full (empty) symbols represent the $\alpha = \frac{1}{2}$ ($-\frac{1}{2}$) signatures of the bands.

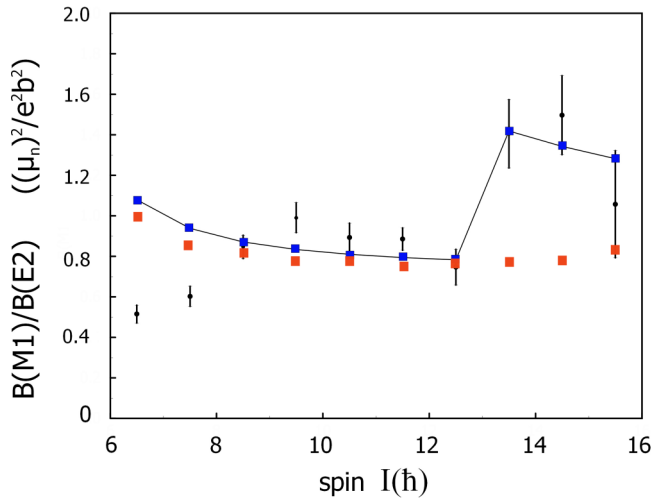FIG. 7. Experimental and calculated $B(M1)/B(E2)$ ratios (in units of μ_N^2/e^2b^2) as a function of spin $I(\hbar)$ for the $7/2^-$[523] rotational sequence of ^{167}Tm. Experimental values are represented by filled circles with their associated error bars. The red squares correspond to $B(M1)/B(E2)$ values calculated using the semiclassical cranking formula of Dönau and Frauendorf [33,34] in which the experimental quasiparticle alignments were used. The theoretical values presented as blue squares, joined by lines to guide the eye, correspond to a similar calculation in which the neutron quasiparticle alignment is assumed to be zero for spin values up to $25/2\hbar$ and $7\hbar$ for spins above this value. See text for further details.

[33,34], namely

$$\frac{B(M1, I \rightarrow I-1)}{B(E2, I \rightarrow I-2)}$$

$$= \frac{12}{5\,Q_0^2 \cos^2(30° + \gamma)}\left(1 - \frac{K^2}{(I-\frac{1}{2})^2}\right)^{-2} K^2$$

$$\times \left[(g_p - g_R)\left(\sqrt{1 - \frac{K^2}{I^2}} - \frac{i_p}{I} \pm \frac{\Delta e'}{\hbar\omega}\right) - (g_n - g_R)\frac{i_n}{I}\right]^2,$$

where i_p and i_n are the proton and neutron aligned angular momenta. In the frequency range populated, the change in alignment is attributed entirely to the aligning quasineutrons; the value of i_p is assumed to be constant and here is set to 0.8 $\hbar$. The g factors associated with collective rotation, the single quasiproton, and the aligning quasineutrons are denoted by g_R, g_p and g_n, respectively. The values of g_p and g_R for the $7/2^-$[523] Nilsson state were obtained from Ref. [36] and are 1.39 and 0.48 respectively and, for spins above the backbend, the value of g_n, characteristic for $i_{13/2}$ neutrons, was taken to be -0.2 [37]. The value of K was assumed to remain constant with rotation and, as the $7/2^-$[523] rotational sequence is axially symmetric, γ was set to zero. The experimental signature splitting can be seen to be negligible, Fig. 6, and therefore $\frac{\Delta e'}{\hbar\omega}$ were also set to zero. In order to normalize the theoretical fit to the experimental data the value of electric quadrupole moment squared (Q_0^2) was taken to be 48 e^2b^2. In the first comparison of the $B(M1)/B(E2)$ values calculated using the formula of

Dönau and Frauendorf with the experimental values, the value of i_n was set to $0\hbar$ up to spin values of up to $25/2\hbar$ and $7\hbar$ for spins above this value, corresponding to the full alignment gained after the AB band crossing in the even-even core. The simple theoretical estimates can be seen to reproduce the trend of the experimental results reasonably well. In the second calculation, the values of neutron quasiparticle alignment were taken from the experimental values of Fig. 6(b); the calculations do not reproduce the increase in $B(M1)/B(E2)$ values above spin $25/2\hbar$, which, for such a comparison, is unusual. Again, It would be helpful to extend this rotational sequence in ^{167}Tm well beyond the rotational frequency corresponding to the full alignment of the two $i_{13/2}$ quasineutrons in order to study the evolution of $B(M1)/B(E2)$ values with increasing angular momentum.

F. Comparison with the results of the projected shell model

The projected shell model (PSM) [38] is a shell-model configuration mixing method that constructs its model basis from angular-momentum projected multiquasiparticle (qp) states. The model was established in the early 1990s by Hara and one of the present authors (YS) aiming at describing rotational bands in well-deformed nuclei. The present nucleus ^{167}Tm belongs to the mass region where odd-mass nuclei were first discussed by the model [39]. It was shown [40] that the model can well describe signature splitting effects in odd proton nuclei. Later, the PSM was successfully applied to various isotopes to interpret high-spin rotational bands in deformed odd-proton nuclei (see Refs. [41–43] for example). The PSM employs the Nilsson potential to generate deformed single particle states. Pairing correlation is included through a BCS calculation. The violated angular-momentum quantum number in the deformed quasiparticle states (for both protons and neutrons) is recovered by the angular-momentum-projection technique. Therefore, in the PSM the theoretical results can be compared level to level with experimental data, for example those presented in Fig. 1 of the present article, without the need of transforming the data to the Routhian frame. For details of the PSM, we refer to the recent review article [44].

To generate realistic deformed single-particle states for ^{167}Tm, we use the newly adjusted Nilsson parameters [45]. We employ $\epsilon_2 = 0.280$ and $\epsilon_4 = 0.015$ as the input deformation parameters, which are the values indicated by total Routhian surface calculations. The monopole-pairing strength is taken to be $G_M = [G_1 \mp G_2(N - Z)/A]/A$, with "$-$" for neutrons and "$+$" for protons, and $G_1 = 20.12$ and $G_2 = 13.13$. The quadrupole-pairing strength G_Q is assumed to be proportional to G_M with the proportionality constant fixed at 0.20. These parameters are standard for PSM calculations for rare earth nuclei [38].

In Fig. 8, the excited states of the four rotational bands in ^{167}Tm are plotted and compared with the current experimental data presented in Fig. 1. The dominant configuration for each rotational band is labeled in the plots. The observed basic feature, namely the "zigzag" behavior within the bands in (a) and (c) and the absence of "zigzags" in (b) and (d), is correctly described. The phase of the "zigzags" follows the rule [39,40] of signature splitting in band energies such that a state is
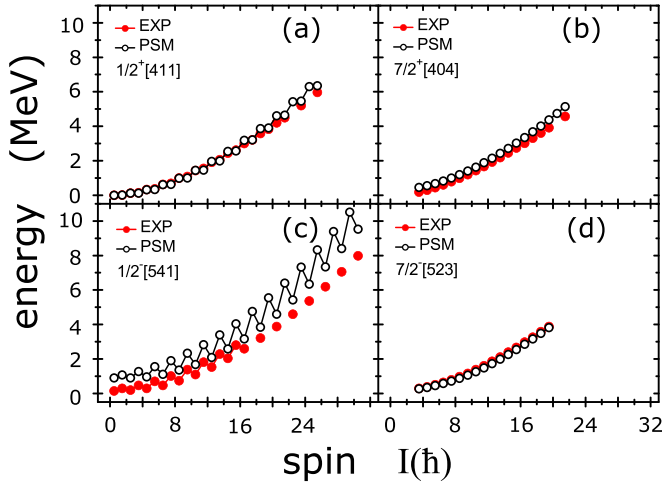
FIG. 8. Comparison of experimental and calculated band structures for ^{167}Tm. See text for details.

FIG. 9. Energy levels for the excited bands of ^{167}Tm, calculated with two different sets of deformation parameters. See text for details.

favored (unfavored) in energy if $I - j =$ even (odd), with I being the spin of a state in the rotational band and j the total angular momentum of the spherical limit for the configuration to which the band is assigned.

The calculated $1/2^+[411]$ ground state band is found to be in excellent agreement with the experimental data with small-amplitude zigzags, as seen in Fig. 8(a). The Nilsson state belongs to the proton $2d_{3/2}$ orbital in the spherical limit, and according to the signature splitting rule, the energy states with spin 3/2, 7/2, 11/2, ... ($I - 3/2 =$ even) are favored. This trend is correctly reproduced by the calculation. In Figs. 8(b) and 8(d), good agreement of calculations with the data is also achieved for the rotational bands assigned as $7/2^+[404]$ and $7/2^-[523]$. These are high-K bands, and therefore, do not exhibit zigzags in band energies.

In Fig. 8(c), the $1/2^-[541]$ band corresponds to the intrinsic 1-qp configuration with $K = 1/2$ of the $1h_{9/2}$ orbital. Due to the high-j, low-K nature, this band exhibits strong signature splitting in band energies. According to the signature splitting rule, the energy states with spin 1/2, 5/2, 9/2, ... ($I - 9/2 =$ even) are favored in energy. While this feature is correctly reproduced by the calculation, the theoretical curve in Fig. 8(c) is shifted higher in energy compared to the data and the zigzag behavior is exaggerated.

In order to probe the sensitivities of the calculated energy levels to the choice of deformation parameters, additional calculations were performed using two more sets of input quadrupole deformation parameters for the $1/2^-[541]$ and $7/2^+[404]$ bands. In Fig. 9, the label PSM1 refers to a calculation with a larger $\varepsilon_2 = 0.315$ and $\varepsilon_4 = 0.013$ values, while PSM2 corresponds to a calculation with smaller values, namely $\varepsilon_2 = 0.265$ and $\varepsilon_4 = 0.013$. The other calculation conditions remained unchanged. It is found that, for the calculation with PSM1, the energy levels of the $1/2^-[541]$ band agree much better with the data. In the Nilsson diagram, the $1/2^-[541]$ 1-qp state becomes an important excited state in the $\varepsilon_2 = 0.300$–0.350 deformation region. In contrast, for the positive-parity $7/2^+[404]$ band, the energy levels can be reproduced perfectly with the smaller deformation of PSM2.
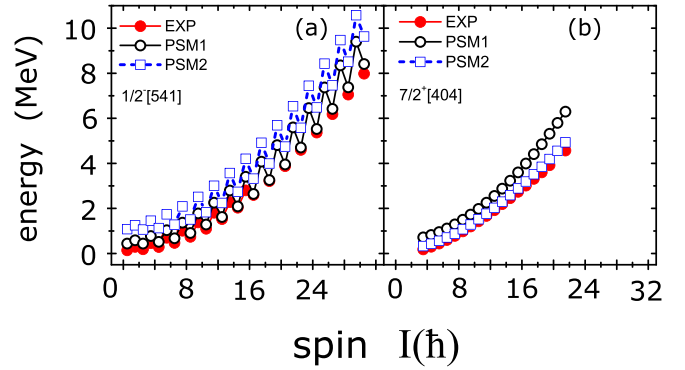
It may therefore be concluded that the calculated energy levels of the 1-qp bands in ^{167}Tm depend sensitively on the deformation parameters. Reference [46] reached a similar conclusion.

V. SUMMARY

The ^{164}Dy(^{7}Li, $4n\gamma$)^{167}Tm fusion-evaporation reaction was used in the present work in a study of the rotational sequences of ^{167}Tm. The $1/2^-[541]$ yrast sequence has been established to spin $61/2^-$, the $1/2^+[411]$ ground-state band extended to $(51/2^+)$, and the $7/2^+[404]$ and $7/2^-[523]$ rotational sequences extended to spins $(43/2^+)$ and $(39/2^-)$, respectively. Previously unassigned spin and parity assignments should be regarded as tentative. Experimental Routhians and quasiparticle aligned angular momenta have been discussed within the context of the cranked shell model. For the rotational sequence based on the $1/2^+[411]$ Nilsson configuration, there is an observed signature dependence of rotational frequency at which the decay sequences based on the three-quasiparticle configuration cross the sequences based on the one quasiproton configuration; this is a consequence of the signature splitting of the single-quasiparticle Routhians. The experimental crossing frequencies are in good agreement with the results of CSM calculations. No extensions to the published level scheme were possible for for the rotational sequence based on the $1/2^-[541]$ configuration. There is no experimental evidence that the deformation-driving properties of the $7/2^+[404]$ orbital has resulted in the crossing frequency being significantly different from that of the yrast sequence of the ^{166}Er core. For the decay sequences based on the $7/2^-[523]$ configuration, a comparison of experiment with the results of CSM calculations is challenging; in this case, the strong interaction between the one- and three-quasiparticle decay sequences results in Routhians for which it is difficult to determine the crossing frequency within the normal ≈ 2 keV uncertainty. Similarly, the quasiparticle alignment increases over the complete measured range of rotational frequencies. The theoretical estimates of $B(M1)/B(E2)$ ratios as a function of spin $I(\hbar)$ for the $7/2^-[523]$ rotational sequence, based on the semiclassical cranking formula of Dönau and Frauendorf [33,34], have been shown to

reproduce the trend of the experimental results reasonably well when the value of the $i_{13/2}$ neutron quasiparticle alignment was set to $0\hbar$ up to spin values of up to $25/2\hbar$ and $7\hbar$ for spins above this value, corresponding to the full CSM alignment gain after the AB band crossing. However, when the values of neutron quasiparticle alignment were taken from experiment, the calculations do not reproduce the increase in $B(M1)/B(E2)$ values above spin $25/2\hbar$ which, for such a comparison, is unusual. It would be helpful to extend this rotational sequence well beyond the rotational frequency corresponding to the full alignment of the two $i_{13/2}$ quasineutrons in order to study the evolution of $B(M1)/B(E2)$ values with increasing angular momentum. Finally, the excited state predictions of the projected shell model (PSM) are in excellent agreement with the experimental data over the complete range of spin values. In particular, the experimental signature splitting of the low-Ω $1/2^+[411]$ ground-state and $1/2^-[541]$ bands is correctly described. For the rotational sequences based on the $1/2^-[541]$ configuration, the theoretical curve is

shifted higher in energy compared to the data and the "zigzag" behavior is exaggerated. It is found that the calculated energy levels of the $1/2^-[541]$ band agree much better with the data when a larger value of the quadrupole deformation parameter is used. It may be concluded that the calculated energy levels of the 1-qp bands in ^{167}Tm depend sensitively on the deformation parameters used in the PSM calculation.

ACKNOWLEDGMENTS

[1] H. J. Jensen, R. A. Bark, P. O. Tjøm, G. B. Hagemann, I. G. Bearden, H. Carlsson, S. Leoni, T. Lönnroth, W. Reviol, L. L. Riedinger, H. Schnack-Petersen, T. Shizuma, X. Z. Wang, and J. Wrzesiński, Nucl. Phys. A **695**, 3 (2001).

[2] T. Tamura, I. Rezanka, S. Iwata, J. O. Rasmussen, and J. Alonso, Phys. Rev. C **8**, 2425 (1973).

[3] C. Foin, S. André, and D. Barneoud, Phys. Rev. Lett. **35**, 1697 (1975).

[4] S. J. Mannanal, B. Boschung, M. W. Carlen, J.-Cl. Dousse, S. Drissi, P. E. Garrett, J. Kern, B. Perny, Ch. Rhême, J. P. Vorlet, C. Günthe, J. Manns, and U. Müller, Nucl. Phys. A **582**, 141 (1995).

[5] M. A. Cardona, D. Hojman, M. E. Debray, A. J. Kreiner, M. Davidson, J. Davidson, D. R. Napoli, D. Bazzacco, N. Blasi, S. M. Lenzi, G. Lo Bianco, and C. Rossi Alvarez, Phys. Rev. C **66**, 044308 (2002).

[6] P. Taras, D. Ward, H. R. Andrews, J. S. Geiger, R. L. Graham, and W. McLatchie, Nucl. Phys. A **289**, 165 (1977).

[7] Md. A. Asgar, T. Roy, G. Mukherjee, A. Dhal, Soumik Bhattacharya, S. Bhattacharyya, C. Bhattacharya, S. Bhattacharya, A. Chaudhuri, K. Banerjee, S. Kundu, S. Manna, R. Pandey, J. K. Meena, R. Palit, S. Biswas, S. Saha, J. Sethi, P. Singh, and D. Choudhury, Phys. Rev. C **95**, 031304(R) (2017).

[8] M. A. Riley, T. B. Brown, N. R. Johnson, Y. A. Akovali, C. Baktash, M. L. Halbert, D. C. Hensley, I. Y. Lee, F. K. McGowan, A. Virtanen, M. E. Whitley, J. Simpson, L. Chaturvedi, L. H. Courtney, V. P. Janzen, L. L. Riedinger, and T. Bengtsson, Phys. Rev. C **51**, 1234 (1995).

[9] J. Gascon, P. Taras, D. C. Radford, D. Ward, H. R. Andrews, and F. Banville, Nucl. Phys. A **467**, 539 (1987).

[10] S. J. Warburton, R. Chapman, J. Copnell, F. Lidén, A. G. Smith, J. P. Sweeney, D. M. Thompson, S. J. Freeman, G. B. Hagemann, and M. Piiparinen, Nucl. Phys. A **591**, 323 (1995).

[11] H. J. Jensen, G. B. Hagemann, P. O. Tjøm, S. Frauendorf, A. Atac, M. Bergström, A. Bracco, A. Brockstedt, H. Carlsson, P. Ekström *et al.*, Z. Phys. A **340**, 351 (1991).

[12] N. S. Pattabiraman, Y. Gu, S. Frauendorf, U. Garg, T. Li, B. K. Nayak, X. Wang, S. Zhu, S. S.Ghugre, R. V. F. Janssens *et al.*, Phys. Lett. B **647**, 243 (2007).

[13] R. Bengtsson, I. Hamamoto, and B. Mottelson, Phys. Lett. B **73**, 259 (1978).

[14] M. J. Burns, R. Chapman, K. M. Spohr, J. Ollier, M. Labiche, X. Liang, E. Farnea, M. Axiotis, T. Martinez, D. R. Napoli, C. A. Ur, and Th. Kröll, J. Phys. G: Nucl. Part. Phys. **31**, S1827 (2005).

[15] A. Fitzpatrick, S. Y. Araddad, R. Chapman, J. Copnell, F. Lidén, J. C. Lisle, A. G. Smith, J. P. Sweeney, D. M. Thompson, W. Urban *et al.*, Nucl. Phys. A **582**, 335 (1995).

[16] H. J. Jensen, R. A. Bark, R. Bengtsson, G. B. Hagemann, P. O. Tjøm, S. Y. Araddad, C. W. Beausang, R. Chapman, J. Copnell, A. Fitzpatrick, S. J. Freeman, S. Leoni, J. C. Lisle, J. Simpson, A. G. Smith, D. M. Thompson, S. J. Warburton, and J. Wrzesiński, Z. Phys. A **359**, 127 (1997).

[17] D. Bazzacco *et al.*, in *Proceedings of the Conference on Nuclear Structure at High Angular Momentum, Ottawa, 1992* (AECL, Ottawa, 1992), p. 10613.

[18] C. R. Alvarez, Nucl. Phys. News **3**, 10 (1993).

[19] A. G. Smith, University of Manchester (private communication).

[20] D. C. Radford, Nucl. Instrum. Methods Phys. Res., Sect. A **361**, 297 (1995).

[21] S. Olbrich, V. Ionescu, J. Kern, and C. Nordmann, Nucl. Phys. A **342**, 133 (1980).

[22] L.-G. Svensson, H. Solhed, N.-G. Jonsson, S. M. Darwish, and J. Lindskog, Phys. Scr. **13**, 193 (1976).

[23] Coral M. Baglin, Nucl. Data Sheets **90**, 431 (2000).

[24] S. Drissi, A. Bruder, J.-Cl. Dousse, V. Ionescu, J. Kern, J.-A. Pinston, S. Andrë, D. Barnéoud, J. Genevey, and H. Frisk, Nucl. Phys. A **451**, 313 (1986).

[25] R. Bengtsson and S. Frauendorf, Nucl. Phys. A **314**, 27 (1979).

[26] R. Bengtsson and S. Frauendorf, Nucl. Phys. A **327**, 139 (1979).

[27] M. J. Burns, R. Chapman, K. M. Spohr, J. Ollier, M. Labiche, X. Liang, E. Farnea, M. Axiotis, T. Martinez, D. R. Napoli, C. A. Ur, and Th. Kröll (unpublished).

[28] R. Bengtsson, S. Frauendorf, and F.-R. May, At. Data Nucl. Data Tables **35**, 15 (1986).

[29] S. G. Nilsson, C. F. Tsang, A. Sobiczewski, Z. Szymański, S. Wycech, C. Gustafson, I-L. Lamm, P. Möller, and B. Nilsson, Nucl. Phys. A **131**, 1 (1969).

[30] A. Bohr and B. R. Mottelson, *Nuclear Structure, Single Particle Motion* (Benjamin, New York, 1975), Vol. 1.

[31] Y.-J. Ma, Z.-H. Li, Y.-Z. Liu, G.-Y. Zhao, J.-B. Lu, Z.-K. Wang, L.-C. Yin, H.-B. Sun, J.-D. Huo, X.-G. Wu, S.-X. Wen, and C.-X. Yang, J. Phys. G: Nucl. Part. Phys. **26**, 43 (1999).

[32] J. Simpson, M. A. Riley, J. R. Cresswell, D. V. Elenkov, P. D. Forsyth, G. B. Hagemann, D. Howe, B. M. Nyako, S. Ogaza, J. C. Lisle, and J. F. Sharpey-Schafer, J. Phys. G: Nucl. Part. Phys. **13**, 847 (1987).

[33] F. Dönau and S. Frauendorf, in *Proceedings of the Conference on High Angular Momentum Properties of Nuclei, Oak Ridge, 1982* (Harwood, New York, 1983), p. 143.

[34] F. Dönau, Nucl. Phys. A **471**, 469 (1987).

[35] P. Frandsen, R. Chapman, J. D. Garrett, G. B. Hagemann, B. Herskind, C.-H. Yu, K. Schiffer, D. Clarke, F. Khazaie, J. C. Lisle, J. N. Mo, L. Carlén, P. Ekström, and H. Ryde, Nucl. Phys. A **489**, 508 (1988).

[36] H. Hübel, Fortschr. Phys. **25**, 327 (1977).

[37] S. Frauendorf, Phys. Lett. B **100**, 219 (1981).

[38] K. Hara and Y. Sun, Int. J. Mod. Phys. E **4**, 637 (1995).

[39] K. Hara and Y. Sun, Nucl. Phys. A **537**, 77 (1992).

[40] Y. Sun, D. H. Feng, and S. X. Wen, Phys. Rev. C **50**, 2351 (1994).

[41] D. E. Archer, M. A. Riley, T. B. Brown, J. Döring, D. J. Hartley, G. D. Johns, T. D. Johnson, R. A. Kaye, J. Pfohl, S. L. Tabor, J. Simpson, and Y. Sun, Phys. Rev. C **52**, 1326 (1995).

[42] S.-X. Wen, H. Zheng, S.-G. Li, G.-S. Li, G.-J. Yuan, P.-F. Hua, P.-K. Weng, L.-K. Zhang, P.-S. Yu, C.-X. Yang, H.-B. Sun, Y.-B. Liu, Y.-Z. Liu, Y. Sun, and D. H. Feng, Phys. Rev. C **54**, 1015 (1996).

[43] Y.-X. Liu, F.-Q. Chen, S.-Y. Yu, and Y. Sun, Sci. China Phys. Mech. Astron. **58**, 1 (2015).

[44] Y. Sun, Phys. Scr. **91**, 043005 (2016).

[45] Y. X. Liu, C. J. Lv, Y. Sun, and F. G. Kondev, J. Phys. G: Nucl. Part. Phys. **47**, 055108 (2020).

[46] Z.-H. Zhang, M. Huang, and A. V. Afanasjev, Phys. Rev. C **101**, 054303 (2020).